WORLD CONFERENCE ON TIMBER ENGINEERING 2025
BRISBANE, AUSTRALIA
Advancing Timber for the Future Built Environment

INTERLAMINAR SHEAR FAILURE DAMAGE EVOLUTION PROCESS OF CLT BASED ON ACOUSTIC EMISSION TECHNOLOGY ANALYSIS

Haiqing Ren[1], Jialei Qu[2], Yinchun Gong[3]

ABSTRACT: Cross laminated timber (CLT) is recognized as alternative to traditional construction materials. In this study, CLT is prepared by the plantation Chinese fir using one component polyurethane. Acoustic emission technology is used to evaluate the damage evolution and failure mode of CLT interlayer shear during load process. The variation of acoustic emission (AE) energy could accurately reflect the evolution of CLT interlayer shear damage. The results showed that the CLT interlayer shear failure mode is mainly the rolling shear failure of the transverse laminate, and the failure mainly occurs at the wheel position and the wood ray position at the junction of the morning and evening wood. In the deformation stage, the AE energy signal was less, the wood fiber bundle buckling, tensile microcracks start to sprout. In the crack propagation stage, the cumulative energy of AE increased linearly, and the shear crack signals with high RA value and low AF value increased. In the failure stage, AE energy signals form a local peak value, and the fracture form of CLT changes from tension-type failure to tension-shear composite failure.

KEYWORDS: Cross laminated timber, Acoustic emission, rolling shear, interlayer shear strength

1 – INTRODUCTION

Cross-laminated timber (CLT) is a sustainable and innovative engineered wood product composed of orthogonally oriented multilayers of solid-sawn or structural composite materials bonded with structural adhesive[1-2]. CLT presents several advantages, including high bidirectional mechanical strength, good dimensional stability, convenient industrial production, and superior fire resistance[3-4]. Owing to these properties, CLT has been widely used in mass timber structures, such as roof panels, floor panels, and wall elements[5–6]. It exhibits potential as a low-carbon, green building material, and its production is supported by established production lines, demonstration buildings, and standardized systems in China[7-8]. Research on the mechanical properties of CLT and glued laminated timber manufactured from Chinese fir [9-10] has been conducted in China. Using native Chinese tree species to prepare engineered wood products can effectively alleviate the global wood resource shortage and address inefficiencies in using Chinese wood resources.

The mechanical properties of CLT directly determine its safety and efficient application in wooden structures. Thus, numerous studies have focused on bond strength, bending, and rolling shear performance[11-12]. CT preparation allows no adhesive on the same layer of laminates, with a maximum gap of 6 mm. Owing to the gap on the side of the laminates, along with the two-dimensional structure of the orthogonal layup, the middle-layer wood is prone to transverse shear brittle failure under vertical loads. Therefore, interlayer shear strength is a key factor in the mechanical failure of CLT[13]. The evaluation of CLT interlayer shear strength primarily examines macroscopic failure modes and strength indices; meanwhile, research on the microscale aspects is limited, including the location, trend, and types of internal cracks generated by interlayer shear failure. Acoustic emission (AE) uses one or more AE sensors for real-time monitoring of the rapid release of energy within the material under external forces, generating transient electrical signals. These signals can be used to evaluate the internal characteristics of the material, such as damage and defects[14-15]. AE has been employed to assess the mechanical properties of wood and wood composites, such as tensile, bending, and

[1] Haiqing Ren, Department of Wood Mechanics and Timber Structure, Research Institute of Wood Industry, Chinese Academy of Forestry, Beijing, China, 100091, renhq@caf.ac.cn

[2] Jialei Qu, Department of Wood Mechanics and Timber Structure, Research Institute of Wood Industry, Chinese Academy of Forestry, Beijing, China, 100091, qjl950227@163.com

[3] Yinchun Gong, Department of Wood Mechanics and Timber Structure, Research Institute of Wood Industry, Chinese Academy of Forestry, Beijing, China, 100091, gongyingchun@caf.ac.cn

https://doi.org/10.52202/080513-0694

compression; however, the spatial evolution of real-time AE signals in CLT has not been studied in depth. Moreover, AE research has focused on laminates and small defect-free samples, with few studies on large structures or full-size CLT. Therefore, analyzing AE signal characteristics is crucial for monitoring the structural integrity and safety of CLT.

In this study, CLT was prepared using Chinese fir and one-component polyurethane. The mechanism governing the influence of laminate grade and gap width on the interlayer shear strength of CLT was analyzed. The microstructural failure characteristics of interlayer shear in CLT were analyzed using scanning electron microscopy. Moreover, the evolution and damage types of interlayer shear failure crack in CLT under vertical loading within the plane were evaluated using AE technology.

2 – EXPERIMENTAL SETUP

2.1 MATERIAL

Chinese fir (Cunninghamia lanceolata) was harvested from Guizhou Province at an average age of 24 y. The logs, with diameters ranging from 250 mm to 320 mm and a length of 3 m, were cut into laminates measuring 3950 mm (length) × 140 mm (width) × 30 mm (thickness). The average kiln-dried density and moisture content of the Chinese fir were 362 kg/m^3±76 kg/m^3 and 10.48%±1.1%, respectively. A total of 864 laminates were graded based on the nondestructive dynamic bending elastic modulus (Ed), using the FAKOPP stress wave method. The average Ed values for laminates in Classes A, B, and C were 13.52, 11.16, and 9.23 GPa, with coefficients of variation equal to 8.62%, 7.34%, and 9.67%, respectively. The CLT specimens were fabricated using a one-component polyurethane adhesive from Henkel Adhesive Co., Ltd. The adhesive, an amber viscous fluid, had a solid content of 100%, a density of 1.16 g/cm^3, and a viscosity range of approximately 2750–4250 mPas.

2.2 CLT SPECIMEN PREPARATION

Five types of CLT with varying layers were manufactured (Table 1). CLT with these five different configurations was manufactured on an industrial CLT production line at Penglai Zhengtai Wood Co., Ltd. A one-component polyurethane adhesive was applied evenly to one face at 180 g/m^2. A pressure of 1.2 MPa was applied to the specimens for 3 h in a 25 ℃ environment. The dimensions (length × width × thickness) of the three-layer CLT were 3950 mm × 1950 mm × 90 mm, and those of the five-layer CLT were 3950 mm × 1950 mm × 150 mm. For each type of CLT, two specimens were prepared, for a total of 10 specimens.

Table 1: Sizes of five CLT types with different layups

Type	Parallel layer	Vertical layer	Number of layer
C_B	Class B	Class C	3
C_A	Class A	Class C	3
C_A2	Class A	Class C	3
C_A4	Class A	Class C	3
5C_A	Class A	Class C	5

2.3 INTERLAYER SHEAR TEST OF CLT CONDUCTED USING AE ANALYSIS

In accordance with ANSI/APA PRG 320-2019 (Standard for Performance-Rated Cross-laminated Timber), three-point bending tests were conducted to evaluate the interlayer shear strength of CLT. The specimens were loaded at a rate of 5 mm/min until failure. The span-to-depth ratio of the specimens was 6. Interlayer shear strength (τ_CLT) in CLT was derived from Equation (1):

$$\tau_{CLT} = k \times \frac{3P}{4bh} \tag{1}$$

where P is the maximum load (N), b is the specimen width (mm), h is the specimen thickness (mm), and k is the correction factor. The k value for three-layer CLT is 0.92, and that for five-layer CLT is 0.81.

AE signal acquisition was performed using two PXR15 resonant sensors with a frequency of 150 kHz (R1 and R2). The threshold voltage of the system was set to 50 dB, the sampling frequency was 2.5 MHz, and the sampling length of a single signal was 16 k. During the test, the universal mechanical testing machine and the AE signal acquisition system were opened synchronously until the specimen was damaged.

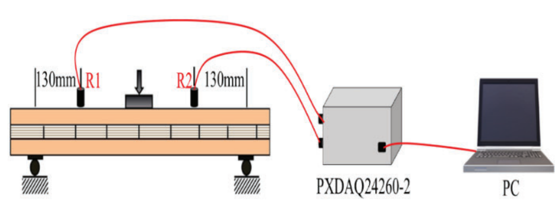

Figure 1. Arrangement of AE sensors in interlaminar shear performance testing of CLT

3 –RESULTS

3.1 INTERLAYER SHEAR STRENGTH IN CLT

https://doi.org/10.52202/080513-0694

Table 2 presents the interlayer shear strength of CLT under different layup structures and gap widths calculated based on Equation 1. The C_A group exhibited an interlayer shear strength of 2.27 MPa, which was 5.11% higher than that of the C_B group; however, no significant difference was found. The reason was that the vertical layers of both C_A and C_B groups consisted of "Class-C" Chinese fir laminate, and the CLT interlayer shear failure primarily involved rolling shear failure in the vertical layer (Fig. 2). Thus, no significant difference in interlayer shear strength was found between the C_A and C_B groups. When the gap of the parallel layer rose from 0 to 4 mm, the C_A2 and C_A4 groups exhibited interlayer shear strengths of 2.20 and 2.10 MPa, which were reduced by 3.19% and 8.10%, respectively. When the gaps between the parallel layers increased, laminate slip in the vertical layer occurred, owing to reduced tensile support from the parallel layers, leading to a significant decrease in interlayer shear strength [16–17]. The $5C_A$ group had an interlayer shear strength of 1.41 MPa, which was 37.88% lower than that of the C_A group. This difference was mainly due to the defects in the "Class-C" laminate itself and the widening of the range of rolling shear failure in the vertical layer as the number of CLT layers increased.

Table 2: Interlaminar shear strength, moisture content, and density along the strong axis of CLT

Type	Interlaminar shear strength	Average moisture content/%	Density g/cm^3
C_B	2.16^{ab}	9.06	0.417
C_A	2.27^{a}	8.06	0.408
C_A2	2.20^{ab}	8.41	0.411
C_A4	2.10^{b}	8.49	0.418
$5C_A$	1.41^{c}	8.54	0.408

The interlayer shear failure modes of CLT were mainly rolling shear failure in the vertical layer and tensile fracture in the bottom layer (Fig. 2). The mechanism underlying interlaminar shear failure in CLT can be further explored from the perspective of wood cell structure. The rolling shear failure in the vertical layer mainly occurred at the earlywood–latewood interface (Figs. 2a–2c), with discontinuous failure along the direction of the wood rays (Fig. 2d). This occurrence was attributed to the lower strength of earlywood cells than that of latewood cells, prompting the occurrence of wood shear failure in or near the earlywood cells[18]. In addition, failure occurred along the wood rays because the tensile strength along the direction of wood rays was lower than that of the adjacent wood fibers[19].

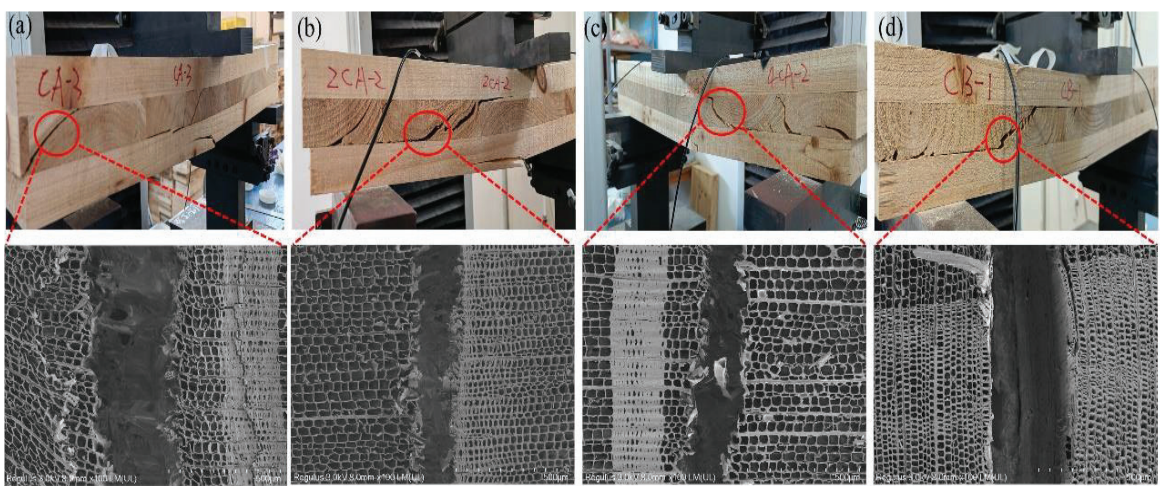

Figure 21. Interlayer shear failure modes of CLT and SEM images.

3.2 ACOUSTIC EMISSION ANALYSIS

The time, load, and energy parameters were selected to analyze the characteristics of AE signals collected during specimen loading. The diagram of AE signal processing is presented in Fig.3. CLTs with different layup structures exhibited a similar AE signal process during interlayer shear. The CLT sample from the C_A group was selected as an example to analyze the characteristics of the AE signals (Fig. 3). The AE energy release during CLT interlayer shear failure can be divided into three stages as the specimen is loaded: (1) During the deformation period (0–35 s), the interlayer shear deformation of the CLT specimen was minimal, and the load curve remained linear. The AE energy of the

https://doi.org/10.52202/080513-0694

specimen was at a low-amplitude stage, indicating that the degree of damage was minimal. The energy release signal was received around 32 s, indicating the occurrence of microcrack initiation inside the specimen. The AE signal at this stage was mainly attributed to the closure of the original defects in the fir CLT specimen caused by the compression from the indenter of the testing machine. (2) During the crack propagation period (35–100 s), small amplitude oscillations appear in the AE energy curve, and irreversible microscopic damage gradually develops within the specimen. Under continuous load, buckling of the wood fiber bundle was intensified, causing microcracks between the cellular or cell wall layers and resulting in significant AE. As irreversible microscopic damage accumulates in the early stage and nascent cracks initiate and expand, the energy released by AE rises linearly, accompanied by cracking sounds. (3) During the failure period (after 100 s), when the specimens reached their ultimate load, significant brittle rolling shear failure occurred. The accumulated AE energy showed a linear mutation, forming a local peak, whereas the internal microcracks in CLT evolved into rolling shear failure in the macroscopic transverse layer.

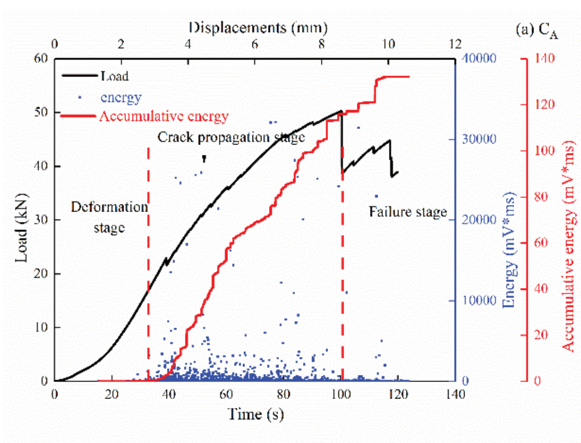

Figure 3. Energy and load time process of CLT.

The classification and identification of cracks in interlayer shear failure were further analyzed by distinguishing the crack types of CLT members on the basis of the RA–AF relationship of AE parameters. In the discrimination method, RA denotes the ratio of rise time to amplitude (us/V), and AF represents the ratio of ringing count to duration (kHz) [20–21]. From the perspective of fracture mechanics, CLT failure cracks are typically categorized into two types: tensile cracks and shear cracks. The RA–AF signal values can be used to classify the cracks that form in CLT under loading (Fig. 4). During the CLT deformation stage (0–35 s) (Fig. 4(a)), tensile cracks with low RA values and high AF values are more prominent on the AF axis side of the main cluster, exhibiting a dense distribution of RA﹣AF points. The compression of CLT samples during this stage leads to the buckling of the wood fiber bundle and the initiation of microcracks. During the crack growth stage (35–100 s, Fig. 4(b)), the overall RA–AF value distribution range expanded further. The CLT crack remained predominantly tensile cracks. However, shear crack signals with high RA and low AF values increased, irreversible shear crack damage gradually developed within the specimen, and new cracks formed and expanded. During the failure stage (after 100 s, Fig. 4(c)), shear crack signals with high RA and low AF values was increased. The internal cracks in the CLT specimens gradually changed from tension to shear cracks, with the shear failure becoming increasingly prominent. The interlaminar shear failure of CLT was characterized by tensile﹣shear fracture.

4 – CONCLUSION

The interlayer shear strength of the C_A group was 2.27 MPa, 5.11% higher than that of the C_B group; no significant difference was indicated. When the gap of the parallel layer was increased from 0 to 4 mm, the interlayer shear strength was reduced by 8.10%. The $5C_A$ group had an interlayer shear strength of 1.41 MPa. Relative to that of the C_A group, its shear strength was reduced by 30.77%, indicating a significant difference.

The interlayer shear failure modes of CLT primarily consisted of rolling shear failure in the vertical layer and tensile fracture in the bottom layer. Rolling shear failure in the transverse laminate predominantly occurred at the junction of earlywood and latewood, particularly at the wheel position and along the wood rays.

The variation in AE energy parameters can accurately reflect the evolution process of CLT interlayer shear damage. During the deformation stage, fewer AE energy signals were observed, with the buckling of the wood fiber bundles under load and the formation of tensile microcracks. During the crack propagation stage, cumulative AE energy increased linearly, accompanied by an increase in shear crack signals with high RA and low AF values. The failure mode of CLT changed from tension-type failure to a tension﹣shear composite failure.

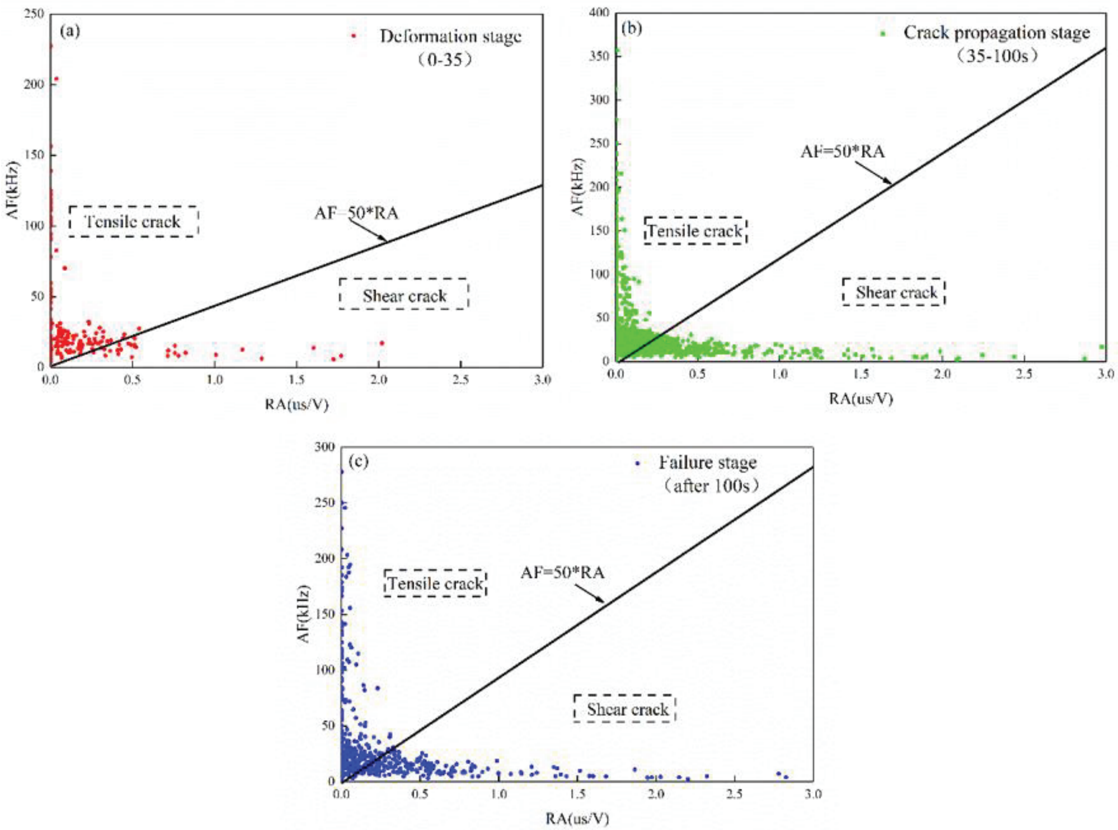

Figure 4. RA–AF distribution in CLT interlayer shear across different stage

5 – REFERENCES

[1] R. Steiger, A. Gülzow, C. Czaderski, M.T. Howald, P. Niemz. "Comparison of bending stiffness of cross-laminated solid timber derived by modal analysis of full panels and by bending tests of strip-shaped specimens." In: European Journal of Wood and Wood Products 70(1-3) (2012) 141-153.

[2] P. Santos, L. Sousa, L. Godinho, J.R. Correia, A. Dias. "Acoustic and thermal behaviour of cross-insulated timber panels." In: Journal of Building Engineering 44 (2021) 103309.

[3] S. Kurzinski, P. Crovella, P. Kremer. "Overview of cross-laminated timber (CLT) and timber structure standards across the world." In: Mass Timber Construction Journal 5(1) (2022) 1-13.

[4] L. Shi, Y. Gong, M. Li, H. Ren, Y. Zhong, Y. Wang. "Gluing parameters optimization and failure mechanism of cross-laminated timber prepared with Chinese fir." In: Industrial Crops and Products 215 (2024) 118640.

[5] H. Song, Z. Wang, Y. Gong, L. Li, J. Zhou, M. Gong. "Low-cycle fatigue life and duration-of-load effect for hybrid CLT fabricated from lumber and OSB." In: Journal of Building Engineering 46 (2022) 103832.

[6] Q. Ye, Y. Gong, H. Ren, L. Peng, H. Zhang. "Theoretical, numerical and experimental studies on thermal insulation performance of different cross laminated timber walls." In: Journal of Building Engineering 72 (2023) 106640.

[7] Y. Gong, S. Xiong, M. Li, Y. Wang, H. Ren, Z. Wang. "Behaviour of hybrid cross laminated timber in compression perpendicular to grain in different layup structure, support conditions, and loading configurations." In: Industrial Crops and Products 200 (2023) 116804.

[8] A. Aloisio, R. Cirella, E. Antonacci, R. Alaggio. "Hypothesis on the Decrement of the First Natural Frequencies of the Santa Maria Di Collemaggio Basilica from Three Years Monitoring: The Role of

https://doi.org/10.52202/080513-0694

the CLT Roof." In: International Journal of Architectural Heritage 17(6) (2023) 955-969.

[9] Q. Li, Z. Wang, Z. Liang, L. Li, M. Gong, J. Zhou. "Shear properties of hybrid CLT fabricated with lumber and OSB." In: Construction and Building Materials 261 (2020) 120504.

[10] M. Li, H. Ren. "Study on the interlaminar shear properties of hybrid cross-laminated timber (HCLT) prepared with larch, poplar and OSB." In: Industrial Crops and Products 189 (2022) 115756.

[11] Z. Wang, H. Fu, M. Gong, J. Luo, W. Dong, T. Wang, Y.H. Chui. "Planar shear and bending properties of hybrid CLT fabricated with lumber and LVL." In: Construction and Building Materials 151 (2017) 172-177.

[12] W.G. Davids, N. Willey, R. Lopez-Anido, S. Shaler, D. Gardner, R. Edgar, M. Tajvidi. "Structural performance of hybrid SPFs-LSL cross-laminated timber panels." In: Construction and Building Materials 149 (2017) 156-163.

[13] Y. Gong, F. Liu, Z. Tian, G. Wu, H. Ren, C. Guan. "valuation of Mechanical Properties of Cross-Laminated Timber with Different Lay-ups Using Japanese Larch." In: Journal of Renewable Materials 7.10 (2019): 941-956.

[14] T. Wang, Q. Huang, Z. Wang, M. Gong. "Rolling shear failure of CLT transverse layer: AE characterization of damage mechanisms under different test methods." In: Construction and Building Materials 440 (2024) 137479.

[15] M. Diakhate, E. Bastidas-Arteaga, R.M. Pitti, F. Schoefs. "Cluster analysis of acoustic emission activity within wood material: Towards a real-time monitoring of crack tip propagation." In: Engineering Fracture Mechanics 180 (2017) 254-267.

[16] Y. Lu, W. Xie, Z. Wang, Z. Gao. "Shear stress and interlaminar shear strength tests of cross-laminated timber beams." In: BioResources 13(3) (2018) 5343-5359.

[17] W. Xie, Y. Ding, Z. Wang, Z. Gao, T. Zhang, Y. Zhou, Y. He, X. Huang. "Testing and analysis of hemlock cross laminated timber." In: Wood Research 65(5) (2020) 819-832.

[18] M. Musah. "Bonding hardwood lumber for cross laminated timber: Properties and environmental impacts." In: Michigan Technological University, 2020.

[19] G. Bingxin, L. Huangfei, X. Bin. "Study on the influence of wood ray morphological characteristics on the tensile strength of wood parallel to grain." In: Industrial Crops and Products 221 (2024) 119258.

[20] M. Liu, J. Lu, P. Ming, J. Song. "AE-based damage identification of concrete structures under monotonic and fatigue loading." In: Construction and Building Materials 377 (2023) 131112.

[21] W. Liu, W. Zhou, H. Li. "Acoustic emission characteristics of Pykrete under uniaxial compression." In: Cold Regions Science and Technology 202 (2022) 103645.